

Relation between widths of proton resonances and neutron asymptotic normalization coefficients in mirror states of light nuclei in a microscopic cluster model.

N. K. Timofeyuk¹⁾ and P. Descouvemont²⁾

¹⁾ Department of Physics, School of Electronics and Physical Sciences,
University of Surrey, Guildford, Surrey GU2 7XH, England, UK

²⁾ Physique Nucléaire Théorique et Physique Mathématique, CP229
Université Libre de Bruxelles, B1050 Brussels, Belgium

(Dated: November 18, 2018)

It has been suggested recently (*Phys. Rev. Lett.* 91, 232501 (2003)) that the widths of narrow proton resonances are related to neutron Asymptotic Normalization Coefficients (ANCs) of their bound mirror analogs because of charge symmetry of nucleon-nucleon interactions. This relation is approximated by a simple analytical formula which involves proton resonance energies, neutron separation energies, charges of residual nuclei and the range of their strong interaction with the last nucleon. In the present paper, we perform microscopic-cluster model calculations for the ratio of proton widths to neutron ANCs squared in mirror states for several light nuclei. We compare them to predictions of the analytical formula and to estimates made within a single-particle potential model. A knowledge of this ratio can be used to predict unknown proton widths for very narrow low-lying resonances in the neutron-deficient region of the *sd*- and *pf*-shells, which is important for understanding the nucleosynthesis in the *rp*-process.

PACS numbers: 21.10.Jx, 21.60.Gx, 27.20.+n, 27.30.+t

I. INTRODUCTION

Many nuclear reactions occur due to virtual and real decays of nuclear levels. The amplitudes of these decays are important structural characteristics of nuclei and their knowledge is needed to predict reaction cross sections correctly. The decay amplitudes are related in a simple way to the asymptotic normalization coefficients (ANCs) [1, 2]. The latter determine the magnitude of the large distance behaviour of the projections of nuclear wave functions into their decays channels. A growing interest of the nuclear physics community to the ANCs is connected with their applications in nuclear astrophysics.

It has been realised recently that the amplitudes of one-nucleon decays of two mirror nuclear states into mirror-conjugated channels should be related if charge symmetry of NN interactions is valid [3]. As a consequence, the ANCs of a pair of particle-bound mirror states can be linked by an approximate analytical expression, given in Ref. [3], which contains only nucleon separation energies, charges of the product nuclei and the range of the strong interaction between the last nucleon and a core. This link can be used to predict cross sections of non-resonant proton capture if mirror neutron ANCs are known.

In bound-unbound mirror pairs, mirror symmetry of one-nucleon decay amplitudes manifests itself via a link between the width Γ_p of a proton resonance and the ANC C_n of its mirror bound analog [3]. With several assumptions, one of which suggests that mirror nuclei have exactly the same wave functions in the nuclear interior, the ratio

$$\mathcal{R}_\Gamma = \Gamma_p / C_n^2, \quad (1)$$

can be approximated by the expression

$$\mathcal{R}_\Gamma \approx \mathcal{R}_0^{\text{res}} = \frac{\hbar^2 \kappa_p}{\mu} \left| \frac{F_l(\kappa_p R_N)}{\kappa_p R_N j_l(i \kappa_n R_N)} \right|^2 \quad (2)$$

from Ref. [3]. In this expression, l is the orbital momentum, $\kappa_{p(n)} = (2\mu/\hbar^2 \epsilon_{p(n)})^{1/2}$, $\epsilon_{p(n)}$ is the energy of the proton resonance (neutron separation energy), μ is the reduced mass for the last nucleon plus core, F_l is the regular Coulomb waves function, j_l is the spherical Bessel function and R_N is the range of the strong interaction between the last nucleon and the core. Several examples considered in Ref. [3] have shown that for narrow $l \neq 0$ resonances the predictions of formula (2) are close to predictions of a single-particle potential model in which charge symmetry of mirror potential wells and equality of mirror spectroscopic factors are assumed. However, for the broad *s*-wave resonance $^{13}\text{C}(\frac{1}{2}^+)$ these predictions diverged by about 40%. Moreover, for two mirror pairs the ratio $\mathcal{R}_\Gamma^{\text{exp}}$, constructed using measured proton widths and neutron ANCs, deviate from the predictions of both the analytical formula and the single-particle model. Therefore, an improved theoretical understanding of the relation between widths of proton resonances and ANCs of their mirror analogs is required.

A proper understanding of the link between the width of a proton resonance and the neutron ANC of its mirror analog can be important for predicting the rate for a particular class of resonant proton capture reactions at stellar energies. This class includes reactions that proceed via very narrow isolated resonance states the proton width Γ_p of which is either comparable to or much less than its γ -decay width Γ_γ . The capture rates for these reactions, determined by $\Gamma_p \Gamma_\gamma / (\Gamma_p + \Gamma_\gamma)$, depend strongly on Γ_p . Such narrow resonances can be found in the neutron-deficient region of the *sd* and *pf* shells

(for example, some levels in ^{25}Si , ^{27}P , ^{33}Ar , ^{36}K and $^{43,46}\text{V}$) and their study is important for understanding nucleosynthesis in the rp process. For the resonances mentioned above Γ_p can be much less than 1 eV. Direct measurements of such tiny widths using proton elastic scattering are impossible. Proton transfer reactions can be used instead. Their analysis (for example, within the distorted-wave formalism) provide spectroscopic factors which are combined together with single-particle widths to get necessary partial proton widths Γ_p . However, uncertainties in Γ_p extracted using such a procedure are about 50% [4]. These uncertainties arise because of problems in the theoretical treatment of stripping reactions to the continuum and due to uncertainties in prediction of single-particle proton widths.

We suggest an alternative way to determine very small proton widths using the link \mathcal{R}_Γ to the neutron ANC s of their particle-stable mirror analogs. The neutron ANC s C_n can be determined from experiments with transfer reactions to bound states, the theoretical analysis of which encounters less problems than that of stripping to continuum. The neutron ANC s can be determined with typical accuracy of 10 to 20%. If the uncertainties in \mathcal{R}_Γ are less than 10%, then the accuracy of determination of $\Gamma_p = \mathcal{R}_\Gamma C_n^2$ can be between 10 to 30%. This is more accurate than the distorted wave analysis of stripping to continuum can provide. If the determination of C_n requires experiments with stable beams rather than with radioactive beams, then even better accuracy may be achieved.

In this paper, we calculate the ratio \mathcal{R}_Γ for some resonances in ^{8}B , $^{12,13}\text{N}$, ^{23}Al and ^{27}P within a microscopic cluster model (MCM) which is ideally suited for studying decay properties of nuclear levels. In our previous work [5], we used the same model to study mirror symmetry in ANC s for bound states of these nuclei. Our study has confirmed the general trend predicted by the simple analytical formula of Ref. [5] for bound-bound mirror pairs which is similar to Eq. (2). The deviations from this formula were in general less than 7% but could increase up to 12% for loosely bound s -states with a node and for nuclei with strongly excited cores. Here, we compare the calculated ratio \mathcal{R}_Γ to the analytical formula (2) and to estimates obtained within a single-particle potential model on the assumption that single-particle potential wells for mirror states are the same. First of all, we clarify in Sec. II the meaning of Γ_p in formula (2). Then in Sec. III we compare the predictions of this formula with exact two-body calculations. In Sec. IV we explain briefly our microscopic cluster model. In Sec. V we study the ratio \mathcal{R}_Γ in the MCM. In Sec. VI we discuss mirror symmetry in spectroscopic factors in bound-unbound mirror pairs and in Sec. VII we summarise our study and draw conclusions.

II. LINK BETWEEN Γ_p AND MIRROR ANCs

The approximation (2) for \mathcal{R}_Γ has been derived in Ref. [3] on the assumption that $\Gamma_p = (\hbar^2 \kappa_p / \mu) S_p b_p^2$ [2], where S_p is the spectroscopic factor, b_p is the single-particle ANC of the Gamow function describing the proton motion in the resonance state, and that $S_l^{1/2} b_p$ can be represented by an integral containing the wave functions of nuclei A and $A - 1$ and the interaction potential between the proton and $A - 1$. In reality, different definitions for resonance widths exist [6]. These definitions give similar widths for narrow resonances but may diverge for broad resonances. Therefore, before studying relations between the proton resonance widths and the ANC s of their mirror bound analogs it is important to clarify what do we mean here by a width and what kind of a width enters in Eq. (2). We do this in the context of the microscopic R-matrix method that we further use in our numerical calculations.

A. Resonance widths in the R-matrix approach

Let $\Psi_A^{(+)}(\mathbf{k}, \{\mathbf{r}_i\})$ be the wave function of nucleus A above the $(A - 1) + p$ decay threshold with the relative momentum \mathbf{k} in the decay channel. This wave function satisfies the Schrödinger equation

$$H_A \Psi_A^{(+)}(\mathbf{k}, \{\mathbf{r}_i\}) = E_A \Psi_A^{(+)}(\mathbf{k}, \{\mathbf{r}_i\}), \quad (3)$$

where E_A is the total energy of nucleus A . Let $\Psi_{A-1}(\{\mathbf{r}_i\})$ be the wave function of a bound state of nucleus $A - 1$ with the total energy E_{A-1} :

$$H_{A-1} \Psi_{A-1}(\{\mathbf{r}_i\}) = E_{A-1} \Psi_{A-1}(\{\mathbf{r}_i\}) \quad (4)$$

Multiplying Eq. (3) by $\Psi_{A-1}(\{\mathbf{r}_i\})$, Eq. (4) by $\Psi_A^{(+)}(\mathbf{k}, \{\mathbf{r}_i\})$, subtracting them from each other and integrating over coordinates of nucleus $A - 1$, we get

$$\begin{aligned} & (T_{rel} + V_0^{coul}(r) - E) \langle \Psi_{A-1}(\{\mathbf{r}_i\}) | \Psi_A^{(+)}(\mathbf{k}, \{\mathbf{r}_i\}) \rangle \\ &= \langle \Psi_{A-1}(\{\mathbf{r}_i\}) | \sum_{i=1}^{A-1} V_{iA} - V_0^{coul}(r) | \Psi_A^{(+)}(\mathbf{k}, \{\mathbf{r}_i\}) \rangle \end{aligned} \quad (5)$$

where $E = E_A - E_{A-1}$ and T_{rel} is the kinetic energy operator for the relative motion between p and $A - 1$, V_{ij} is the nucleon-nucleon (NN) potential and

$$V_0^{Coul}(r) = \frac{Z_{A-1} e^2}{r} \quad (6)$$

is the Coulomb attraction between two point charges located at distance r . Using the partial wave decomposition of the overlap integral in the left-hand side of Eq. (5),

$$\langle \Psi_{A-1}(\{\mathbf{r}_i\}) | \Psi_A^{(+)}(\mathbf{k}, \{\mathbf{r}_i\}) \rangle = \sum_{lmSM_S M_{A-1} \sigma} 4\pi i^l$$

$$\begin{aligned} & \times (J_{A-1} M_{J_{A-1}} \frac{1}{2} \sigma |SM_S)(lmSM_S|J_A M_{J_A}) \\ & \times \phi_{lS}(k, r) Y_{lm}(\hat{r}) Y_{lm}^*(\hat{k}) \chi_{\frac{1}{2}\sigma}(A), \quad (7) \end{aligned}$$

where $J_i(M_{J_i})$ is the spin (its projection) of nucleus i , l is the orbital momentum and S is the channel spin, and expanding the source term (right-hand side) of the inhomogeneous equation (5),

$$\begin{aligned} & \langle \Psi_{A-1}(\{r_i\}) | \sum_{i=1}^{A-1} V_{iA} - V_0^{coul}(r) | \Psi_A^{(+)}(\mathbf{k}, \{r_i\}) \rangle \\ & = \sum_{lmSM_S M_{J_{A-1}}} 4\pi i^l (J_{A-1} M_{J_{A-1}} \frac{1}{2} \sigma |SM_S) \\ & \times (lmSM_S |J_A M_{J_A}) \mathcal{S}_{lS}(k, r) Y_{lm}(\hat{r}) Y_{lm}^*(\hat{k}) \chi_{\frac{1}{2}\sigma}(A), \quad (8) \end{aligned}$$

where $k = \sqrt{2\mu E/\hbar^2}$ and μ is the reduced mass of proton and $A-1$, we get an inhomogeneous radial equation for the overlap function $\phi_{lS}(k, r)$:

$$(T_l + V_0^{coul}(r) - E) \phi_{lS}(k, r) = -S_{lS}(k, r), \quad (9)$$

where T_l is the kinetic energy operator in the l 'th partial wave. This equation can be solved using the Green's functions technique. In the single channel limit, the regular at the origin solution of Eq. (9) reads

$$\phi_{lS}(k, r) = \frac{F_l(\kappa r)}{\kappa r v^{1/2}} - \int_0^\infty dr' r'^2 \frac{G_l(r, r')}{rr'} \mathcal{S}_{lS}(k, r). \quad (10)$$

Here F_l is the regular Coulomb wave function, $G_l(r, r')$ is the outgoing Green's function for the point charge in the l 'th partial wave and $v = \hbar k/\mu$ is velocity. In Eq. (10), the factor $v^{-1/2}$ is introduced to provide unity flux.

In the vicinity of an isolated narrow resonance the channel wave function $\phi_{lS}(k, r)$ behaves as follows [7]

$$\phi_{lS}(k, r) \approx \frac{\sqrt{\hbar \Gamma_{lS}^0}}{2\kappa} \frac{\phi_{lS}^{BSA}(r)}{E - E_R - \frac{i}{2} \Gamma_{lS}^0}. \quad (11)$$

Eq. (11), called a bound state approximation, contains a square-integrable function $\phi_{lS}^{BSA}(r)$ which is defined within some channel radius a taken outside the range of the nucleon-nucleus interaction. This function has the dimension of a bound state wave function. A similar bound state approximation can be also written for the source term $\mathcal{S}_{lS}(k, r)$:

$$\mathcal{S}_{lS}(k, r) \approx \frac{\sqrt{\hbar \Gamma_{lS}^0}}{2\kappa} \frac{\mathcal{S}_{lS}^{BSA}(r)}{E - E_R - \frac{i}{2} \Gamma_{lS}^0}. \quad (12)$$

In Eqs. (11) and (12), E_R is the (real) energy of the resonance and the width Γ_{lS}^0 is trivially related to the residue γ_{lS}^2 in the R-matrix pole:

$$\Gamma_{lS}^0 = 2\kappa a \gamma_{lS}^2 / |O_l(ka)|^2. \quad (13)$$

Substituting (12) into (10), using the Green's function from Ref. [8]

$$G_l(r, r') = -\frac{2\mu}{\hbar^2 \kappa} F_l(\kappa r_<) O_l(\kappa r_>), \quad (14)$$

where $O_l = G_l + iF_l$ and G_l is the irregular Coulomb wave function, and neglecting the term that contains the integral from r to infinity we can rewrite the wave function (10) at the channel radius $r = a$ as follows:

$$\begin{aligned} \phi_{lS}(k, a) & \approx \frac{i}{2\kappa a v^{1/2}} (I_l(\kappa a) - U_{lS} O_l(\kappa a)), \\ U_{lS} & = 1 + \frac{2i\sqrt{\hbar \Gamma_{lS}^0} \int_0^a dr r F_l(\kappa r) \mathcal{S}_{lS}^{BSA}}{\kappa \hbar^{3/2} (E - E_R - \frac{i}{2} \Gamma_{lS}^0)} \end{aligned} \quad (15)$$

Here $I_l = G_l - iF_l$ and U is the collision matrix. Comparing Eq. (15) with the R-matrix asymptotics of the wave function ϕ_{lS} in the vicinity of the resonance,

$$\begin{aligned} \phi_{lS}(k, a) & \approx \frac{i}{2\kappa a v^{1/2}} \\ & \times \left(I_l(\kappa a) - O_l(\kappa a) \left(1 + \frac{i\Gamma_{lS}^0(E)}{E - E_R - \frac{i}{2} \Gamma_{lS}^0(E)} \right) \right), \end{aligned} \quad (16)$$

we get

$$\Gamma_{lS}^0 \equiv \Gamma_{lS}^0(E_R) = \frac{2\kappa_R}{E_R} \left| \int_0^a dr r F_l(k_R r) \mathcal{S}_{lS}^{BSA}(r) \right|^2, \quad (17)$$

where $k_R = \sqrt{2\mu E_R/\hbar^2}$. The same result can be obtained in a multi-channel case. Thus, the partial proton decay width in the channel lS is determined by an integral that contains the regular Coulomb function of a real argument and a source term corresponding to the square-integrable wave function defined in some restricted region.

B. ANC_s of bound neutron states

If the mirror analog of the proton resonance at energy E_R is a bound state, then the mirror analog of the overlap function $\phi_{lS}(k, r)$ is the radial overlap integral $I_{lS}(r)$ between the mirror wave functions of nuclei A and $A-1$. This overlap asymptotically behaves as follows,

$$r \sqrt{A} I_{lS}(r) \approx -C_{lS} i^l \kappa_n h_l^{(1)}(\kappa_n r), \quad r \rightarrow \infty, \quad (18)$$

where C_{lS} is the ANC, $h_l^{(1)}$ is the Hankel function of the first kind and κ_n is determined by the separation energy ϵ_n of the mirror neutron. The ANC squared C_{lS}^2 is given by the following expression [9]

$$C_{lS}^2 = \frac{4\mu^2}{\hbar^4 \kappa_n^2} \left| \int_0^\infty dr r^2 \kappa_n j_l(ik_n r) \mathcal{S}_{lS}(r) \right|^2 \quad (19)$$

in which j_l is the spherical Bessel function and $\mathcal{S}_{lS}(r)$ is the radial part of the source term defined by the the

left-hand side of expression Eq. (8) in which mirror wave functions of nuclei A and $A-1$ are used and the Coulomb interactions are absent.

The main contribution to the integrals in Eqs. (17) and to Eq. (19) for Γ_{lS}^0 and C_{lS}^2 comes from some internal region $r \leq R_N < a$. If charge symmetry of the NN interactions is valid and the Coulomb differences in the mirror wave functions of the resonance and the mirror bound state in this region can be neglected, then the reasoning of Ref.[3] leads to the analytical formula (2) for the ratio between Γ_{lS}^0 and C_{lS}^2 . This reasoning suggests to replace the Coulomb interaction in Eq. (8) at $r \leq R_N$ by a constant equal to $E_R + \epsilon_n$ and then to remove this interaction from the source term of the proton by changing the function $F_l(k_R r)$ into some modified function. This function is a regular solution of the Schrödinger equation with the constant Coulomb potential and is equal exactly to the spherical Bessel function $j_l(i\kappa_n r)$ times the normalization coefficient $F_l(\kappa_p R_N)/\kappa_p R_N j_l(i\kappa_n R_N)$. As the result, both Γ_{lS}^0 and C_{lS}^2 contain exactly the same integral and their ratio is determined by the above normalization coefficient and the kinematic factor $\hbar^2 \kappa_p / \mu$.

It is important to notice here that Γ_{lS}^0 defined by Eq. (17) is a residue in the R-matrix pole so that the analytical formula (2) actually links this residue and the ANC of the mirror bound analog. If the proton resonance is narrow then Γ_{lS}^0 is approximately equal to the width Γ_{lS} of the peak in the cross sections of the reactions in which this resonance is populated. However, these two widths are not the same. In the particular case of elastic scattering, the width $\Gamma_{lS} \equiv \Gamma_{lS}(E_R)$ that determines the resonant phase shift $\tan \delta_{lS} = \Gamma_{lS}(E)/2(E - E_R)$ is related to Γ_{lS}^0 as follows [10]:

$$\Gamma_{lS} = \Gamma_{lS}^0 (1 + \gamma_{lS}^2 S_l')^{-1} \quad (20)$$

where $S_l = \text{Re}(kaO_l'/O_l)$. If a link between physically observed width Γ_{lS} and the neutron ANC is considered, then Eq. (2) should be modified by the factor of $(1 + \gamma_{lS}^2 S_l')^{-1}$.

III. TWO-BODY MODEL

According to the analytical formula (2), the ratio between the proton width and the ANC squared of its mirror neutron is model-independent. It is determined only by the proton resonance energy, the neutron separation energy and should be the same for any NN potential employed in calculations. We checked this property for the case of the two-body potential model. We considered a family of Woods-Saxon potentials that give some chosen neutron separation energy ϵ_n , and some chosen energy of proton resonance E_p when the Coulomb potential of the uniformly charged sphere was added. This was achieved by simultaneously varying both the depth and the radius of the Woods-Saxon potential at fixed diffusenesses. The actual numerical values of E_p were the same as the

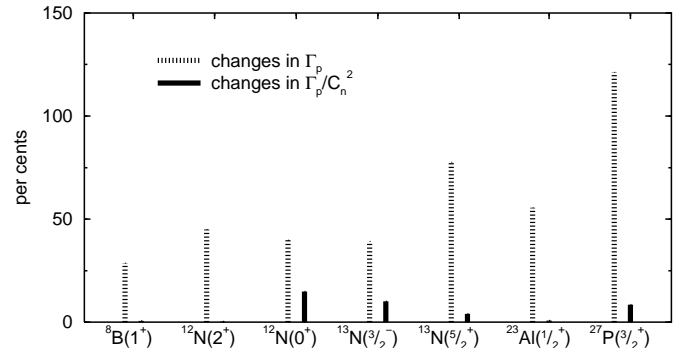


FIG. 1: Changes in proton widths Γ_p and in its ratio to mirror neutron ANC squared Γ_p/C_n^2 with the choice of two-body nuclear potential well for a range of nuclei.

experimental energies of proton resonances in the lowest states ${}^8\text{B}(1^+)$, ${}^{12}\text{N}(2^+, 0^+)$, ${}^{13}\text{N}(\frac{3}{2}^-, \frac{5}{2}^+)$, ${}^{23}\text{Al}(\frac{1}{2}^+)$ and ${}^{27}\text{P}(\frac{3}{2}^+)$. The experimental widths of these resonances are less than 10% of their energy so that the difference between the widths Γ_{lS}^0 and Γ_{lS} should be small. In our two-body calculations, the proton width (which we refer for simplicity as to Γ_p) has been determined from transition of the phase shift via 90° . As for the mirror neutron separation energies ϵ_n , they were the same as those obtained in microscopic calculations below with charge-independent NN interactions.

For different potentials from the same family, the proton widths and mirror neutron ANCs squared changed significantly but in such a way that their ratio was roughly the same. To illustrate this, we have presented in Fig.1 the changes in proton widths by thick vertical dashed lines and the changes in Γ_p/C_n^2 by the vertical solid lines. While Γ_p changes by 30 to 120%, the changes in Γ_p/C_n^2 are much smaller. They are less than 1% for ${}^8\text{B}(1^+)$, ${}^{12}\text{N}(2^+)$ and ${}^{23}\text{Al}(\frac{1}{2}^+)$ and 4% for ${}^{13}\text{N}(\frac{5}{2}^+)$. For ${}^{27}\text{P}(\frac{3}{2}^+)$ the changes in Γ_p/C_n^2 are 8.5% as compared to the 121% changes in Γ_p/C_n^2 . Two other cases, ${}^{12}\text{N}(0^+)$ and ${}^{13}\text{N}(\frac{3}{2}^-)$, are special. Experimentally, these states are seen as narrow resonances with $\Gamma_p/E_p \approx 0.04$. However, they are so narrow only because of their very small single-particle strengths, or spectroscopic factors. In the two-body potential model, the widths of these resonances are about 30 to 50% of the resonance energy, depending on the choice of the two-body potential well. For such broad resonances the definition of the resonance width (17) is not precise anymore and the ratio Γ_p/C_n^2 may behave in a different way. In particular, this ratio is more dependent on the nuclear potential well, 15% for ${}^{12}\text{N}(0^+)$ and 10% for ${}^{13}\text{N}(\frac{3}{2}^-)$, than in the case of the other narrow resonances.

In Fig. 2 we compare the ratio Γ_p/C_n^2 calculated in the two-body model with the analytical estimate \mathcal{R}_0^{res} given by Eq. (2). One can see that \mathcal{R}_0^{res} reproduces very well the general trend in Γ_p/C_n^2 even for the resonance states whose widths are not narrow. The difference between

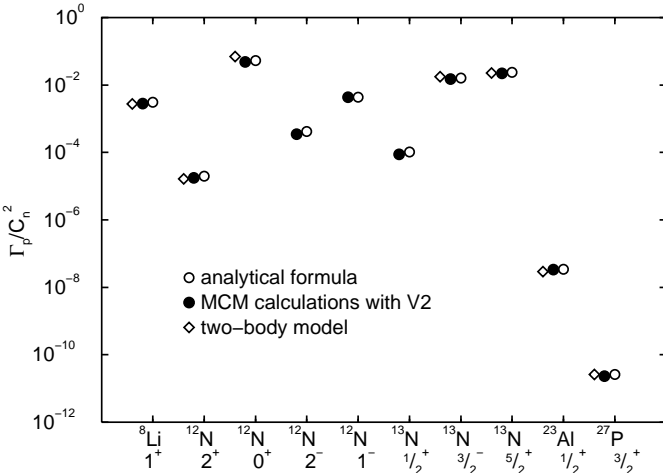


FIG. 2: Ratio of proton width to mirror neutron ANC squared Γ_p^0/C_n^2 (given in units of $\hbar c$) calculated in the two-body potential model, microscopic cluster model and using the analytical formula (2) for a range of nuclei.

Γ_p/C_n^2 and \mathcal{R}_0^{res} does not exceed 30%, being the smallest for the d -wave resonances (less than 3%) and the largest for the wide two-body resonance $^{12}\text{N}(0^+)$ (about 30%).

The weak sensitivity of the ratio of mirror ANCs to the nuclear potentials suggests an alternative empirical way to determine this ratio. If we assume that mirror neutron and proton single-particle wells are exactly the same and that the proton spectroscopic factor S_p can be defined and is equal to the neutron spectroscopic factor and S_n , then the ratio \mathcal{R}_Γ can be approximated by the single-particle ratio $\mathcal{R}_\Gamma^{s.p.}$

$$\mathcal{R}_\Gamma \approx \mathcal{R}_\Gamma^{s.p.} \equiv \Gamma_p^{c.s.}/(b_n^{c.s.})^2, \quad (21)$$

where the proton width $\Gamma_p^{c.s.}$ and the single-particle ANCs $b_n^{c.s.}$ are calculated numerically for exactly the same nuclear potential well. Further below, we compare the results of our microscopic calculations for \mathcal{R}_Γ with the single-particle estimate $\mathcal{R}_\Gamma^{s.p.}$. Such a comparison is useful because unlike \mathcal{R}_0^{res} , $\mathcal{R}_\Gamma^{s.p.}$ takes into account the differences in internal wave functions of mirror nuclei due to the Coulomb interactions.

IV. WAVE FUNCTIONS IN A MICROSCOPIC CLUSTER MODEL

To improve our understanding of \mathcal{R}_Γ we use the microscopic cluster model. The MCM takes into account the differences in the internal structure of mirror nuclei due to the Coulomb interaction and the core excitations effects, which were ignored in the derivation of the analytical formula (2). On the other hand, it also accounts for many-body effects and effects caused by non-diagonal Coulomb couplings, which are absent in the single-particle approximation (21)

The multi-channel cluster wave function for a nucleus A consisting of a core $A - 1$ and a nucleon N can be represented as follows:

$$\Psi^{J_A M_A} = \sum_{lS J_{A-1}\nu} \mathcal{A}[\chi_{\frac{1}{2}\tau} [g_{\nu lS, \omega}^{J_{A-1}}(\mathbf{r}) \otimes [\Psi_\nu^{J_{A-1}} \otimes \chi_{\frac{1}{2}}]_S]_{J_A M_A}] \quad (22)$$

where $\mathcal{A} = A^{-\frac{1}{2}}(1 - \sum_{i=1}^{A-1} P_{i,A})$ and the operator $P_{i,A}$ permutes spatial and spin-isospin coordinates of the i -th and A -th nucleons. In this work, $\Psi_\nu^{J_{A-1}}$ is a wave function of nucleus $A - 1$ with the angular momentum J_{A-1} defined either in translation-invariant harmonic-oscillator shell model, or in a multicluster model. The quantum number ν labels states with the same angular momentum J_{A-1} , S is the channel spin and ω stands for all the quantum numbers that characterise the entrance channel. The function $g_{\nu lS, \omega}^{J_{A-1}}$ also depends on J_A but we omit this index for simplicity.

The relative wave function $g_{\nu lS, \omega}^{J_{A-1}}(\mathbf{r}) = g_{\nu lS, \omega}^{J_{A-1}}(r) Y_{lm}(\hat{r})$ is determined using the microscopic R-matrix method, as explained in detail in Ref. [11]. In this method, the Bloch-Schrödinger equation is solved for the wave function $\Psi^{J_A M_A}$, which allows the correct asymptotic behaviour for the relative wave function $g_{\nu lS, \omega}^{J_{A-1}}$ to be obtained. For particle-unstable states

$$g_{\alpha, \omega}(r) \approx A_\omega \frac{\delta_{\omega\alpha} I_l(\kappa_\nu r) - U_{\omega\alpha} O_l(\kappa_\nu r)}{\kappa_\omega v_\nu^{1/2}}, \quad (23)$$

where I_l and O_l are the ingoing and outgoing Coulomb functions in the channel $\alpha \equiv \{\nu J_{A-1} l S\}$, v_ν is the velocity in this channel and U is the collision matrix. The resonance width Γ_{lS}^0 is determined assuming the Breit-Wigner shape of the collision matrix near an isolated resonance at the energy E_R and the width Γ_{lS} is determined from Γ_{lS}^0 using Eq. (20). As for bound states, the asymptotics of the relative function $g_{\nu lS, \omega}^{J_{A-1}}(r)$ is

$$g_{\nu lS, \omega}^{J_{A-1}}(r) \approx C_{lS, \omega}^{J_{A-1}} \frac{W_{-\eta_\nu, l+1/2}(2\kappa_\nu r)}{r} \quad (24)$$

where $C_{lS, \omega}^{J_{A-1}}$ is the ANC and W is the Whittaker function.

V. RELATION BETWEEN Γ_p AND MIRROR ANCS IN THE MCM

In this section we investigate the ratio \mathcal{R}_Γ for the following $0p$ and sd shell resonances: $^8\text{B}(1^+)$, $^{12}\text{N}(2^+, 1^+, 2^-, 1^-)$, $^{13}\text{N}(\frac{1}{2}^+, \frac{5}{2}^+, \frac{3}{2}^-)$, $^{23}\text{Al}(\frac{1}{2}^+)$ and $^{27}\text{P}(\frac{3}{2}^+)$. The cluster models we used are listed in Table I together with references for further details. The internal structure of these clusters is represented by the shell model Slater determinants composed of the following single-particle oscillator wave functions: $0s$ for

TABLE I: Cluster model for nuclei from the first column. The same model but with mirror-conjugated clusters is used for mirror analogs of these nuclei. For ^{13}N , $2c$ and $4c$ stand for two- and four-cluster model respectively.

Nucleus	Clustering	Core excitations	References
^8B	$(\alpha + ^3\text{He}) + p$ and $(\alpha + p) + ^3\text{He}$	$^7\text{Be}(\frac{1}{2}_{1,2}^-, \frac{3}{2}_{1,2,3,4}^-, \frac{5}{2}_{1,2}^-, \frac{7}{2}_{1,2}^-)$ and $^5\text{Li}(\frac{3}{2}^-, \frac{1}{2}^-)$	[15]
^{12}N	$^{11}\text{C} + p$	$^{11}\text{C}(\frac{1}{2}_{1,2,3}^-, \frac{3}{2}_{1,2,3,4,5,6}^-, \frac{5}{2}_{1,2,3}^-, \frac{7}{2}_{1}^-)$	[16]
$^{13}\text{N}^{2c}$	$^{12}\text{C} + p$	$^{12}\text{C}(0_{1,2,3}^+, 1_{1,2,3}^+, 2_{1,2,3,4,5,6}^+)$	[17]
$^{13}\text{N}^{4c}$	$\alpha + \alpha + \alpha + p$	$^{12}\text{C}(0_{1,2,3}^+, 2_{1,2,3}^+)$	[18]
^{23}Al	$^{22}\text{Mg} + p$	$^{22}\text{Mg}(0_1^+, 1_1^+, 2_{1,2,3}^+, 3_1^+, 4_{1,2}^+)$	[5]
^{27}P	$^{26}\text{Si} + p$	$^{26}\text{Si}(0_1^+, 2_1^+, 4_1^+)$	[5]

α , ^3H and ^3He clusters, $0s$ and $0p$ for the ^{11}B and $^{11,12}\text{C}$ clusters and $0s$, $0p$ and $0d_{\frac{5}{2}}$ for the ^{22}Ne , ^{22}Mg , ^{26}Mg and ^{26}Si clusters. Some excited states of these clusters, appeared in the shell model calculations, are taken into account. They are also listed in Table I. The products of the proton decay and their mirror analogs are always considered to be in their ground states.

We use well adapted effective NN interactions for such calculations, namely, the Volkov potential V2 [12] and the Minnesota (MN) potential [13]. The two-body spin-orbit force [14] and the Coulomb interaction are also included. More details on the conditions of calculations can be found in Ref. [5] and references therein.

Each of V2 and MN have one adjustable parameter that gives the strength of the odd NN potentials V_{11} and V_{33} . To get meaningful values of ANC and proton widths, this parameter should be fitted in each individual case to reproduce the experimental neutron separation energy ϵ_n or the resonance energy E_p of the proton. In most cases, the same choice of the adjustable parameter for mirror states does not let to reproduce exactly ϵ_n and E_p . Therefore, we consider here two cases: (A) We keep the same value of the adjustable parameter for both nuclei of a mirror pair thus imposing charge symmetry of the NN interactions. The value of this parameter is fitted to reproduce experimental value of E_p . (B) We use slightly different adjustable parameters in mirror nuclei to reproduce simultaneously ϵ_n and E_p . This simulates charge symmetry breaking of the effective NN interactions which should be a consequence of the charge symmetry breaking in realistic NN interactions. For both cases we have calculated the ratio $\mathcal{R}_{\Gamma_0}^{MCM} = \Gamma_{lS}^0 / C_{lS}^2$ that we compare to the analytical estimate \mathcal{R}_0^{res} . We have also calculated the ratio $\mathcal{R}_{\Gamma}^{MCM} = \Gamma_{lS} / C_{lS}^2$ which we compare to the single-particle estimate $\mathcal{R}_{\Gamma}^{s.p.}$. In $^8\text{B}(1^+)$ and $^{12}\text{N}(2^+)$, where two different values of the channel spin S are possible, we use the sums $\sum_S \Gamma_{lS}^0$, $\sum_S \Gamma_{lS}$ and $\sum_S C_{lS}^2$ when constructing these ratios.

A. Calculations with charge-independent NN interactions

The calculated ratio $\mathcal{R}_{\Gamma_0}^{MCM}$ for the V2 potential is plotted in Fig.2 together with the prediction \mathcal{R}_0^{res} of the analytical formula (2) and with the single-particle estimate $\mathcal{R}_{\Gamma}^{s.p.}$. As seen in Fig.2, both \mathcal{R}_0^{res} and $\mathcal{R}_{\Gamma}^{s.p.}$ describe very well the general trend in the $\mathcal{R}_{\Gamma_0}^{MCM}$ behaviour.

To see the differences between $\mathcal{R}_{\Gamma_0}^{MCM}$ and \mathcal{R}_0^{res} we have plotted the ratio $\mathcal{R}_{\Gamma_0}^{MCM} / \mathcal{R}_0^{res}$ in Fig.3. The error bars in this figure represent uncertainties in \mathcal{R}_0^{res} due to the choice of R_N . The estimation of these errors is similar to that described in Ref. [5] for bound-bound mirror pairs.

According to Fig.3, the effect of different NN potential choices is normally less than 7% for the $0p$ shell nuclei, being the smallest for the p -wave resonances (less than 2%) and for the d -wave resonance $^{13}\text{N}(\frac{5}{2}^+)$. Slightly bigger effect, about 9%, is seen for the s -wave resonance $^{12}\text{N}(1^-)$. For the sd shell nuclei ^{23}Al and ^{27}P , the sensitivity on the NN potential depends on whether the core excitations are taken into account or not. Without core excitations, the sensitivity to the NN potential choice is less than 6%, which is similar to the case of the $0p$ shell nuclei. When core excitations are present, this sensitivity increases up to 10% for ^{23}Al and 30% for ^{27}P .

Our previous study of ANC in bound-bound mirror pairs [5] has shown that core excitations can be responsible for differences between the MCM calculations for the ratio of mirror ANC and the predictions of the analytical formula (7) of Ref. [3]. In the present paper, we check how important the core excitations are in bound-unbound mirror states. Fig.3 shows the ratio $\mathcal{R}_{\Gamma_0}^{MCM} / \mathcal{R}_0^{res}$ calculated both in the single-channel (no core excitations) and the multi-channel (including the core excitations from Table I) cluster model. One can see that for the $0p$ shell nuclei the results obtained with and without taking core excitations into account differ by no more than 7%. The influence of the core excitations on $\mathcal{R}_{\Gamma_0}^{MCM}$ becomes more important for nuclei in the middle of the sd shell. For ^{23}Al - ^{23}Ne , this influence is 9 - 12%. A similar effect is present in the calculations with the V2 potential for $^{27}\text{P}(\frac{3}{2}^+) - ^{27}\text{Mg}(\frac{3}{2}^+)$. However, for MN, the

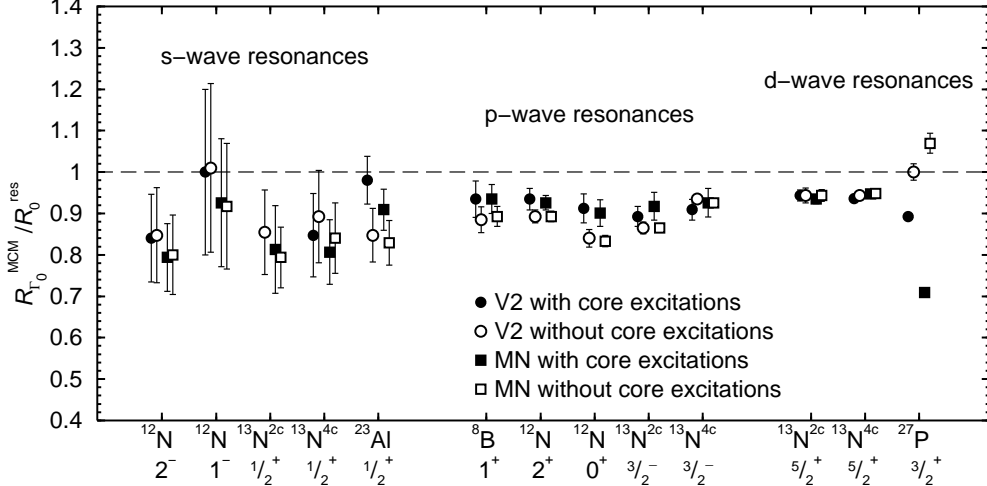


FIG. 3: Ratio between the predictions $\mathcal{R}_{\Gamma_0}^{MCM}$ from the microscopic calculations and the analytical estimate \mathcal{R}_0^{res} of the analytical formula (2). The microscopic calculations are performed for the V2 and MN potentials with and without taking core excitations into account. Charge symmetry of NN interactions is assumed. Both four-cluster ($4c$) and two-cluster ($2c$) calculations for ^{13}N are shown.

influence of core excitations on $\mathcal{R}_{\Gamma_0}^{MCM}$ is much stronger, about 37%. For the MN potential, the d -wave $^{26}\text{Si}(0^+) + p$ configuration in $^{27}\text{P}(\frac{3}{2}^+)$ becomes three times weaker than the s -wave $^{26}\text{Si}(2^+) + p$ configuration. In weak configurations, effects of charge symmetry breaking due to the Coulomb interactions can be more noticeable. In the case of $^{27}\text{P}(\frac{3}{2}^+) - ^{27}\text{Mg}(\frac{3}{2}^+)$, the significant difference between $\mathcal{R}_{\Gamma_0}^{MCM}$ and \mathcal{R}_0^{res} coincides with similar mirror symmetry breaking in the spectroscopic factors of the $^{26}\text{Si}(0^+) + p$ and $^{26}\text{Mg}(0^+) + n$ configurations, which is about 33% for MN. For V2, the d -wave $^{26}\text{Si}(0^+) + p$ configuration dominates and the mirror symmetry breaking for spectroscopic factor of this configuration is only 4%.

The average difference between \mathcal{R}_0^{res} and $\mathcal{R}_{\Gamma_0}^{MCM}$ is about 10%. This is larger than the average deviation between the microscopic calculations with charge-independent NN interactions and the predictions of analytical formula for the ratio of mirror ANC squared for bound-bound mirror pairs, obtained in Ref. [5].

B. Calculations with charge breaking symmetry NN interactions

The calculated ANCs for bound neutron states are shown in Table II. We show them in the lj coupling scheme that is widely accepted in the analysis of transfer reactions, in which these ANCs can, or have been determined. Transition from the lS coupling scheme to the lj coupling scheme is performed using standard technique. For $^8\text{Li}(1^+)$ and $^{12}\text{N}(2^+)$ we also show the sum of the ANCs squared $C_l^2 = \sum_j C_{lj}^2 = \sum_S C_{lS}^2$. We have also calculated the radial part $I_{lj}(r)$ of the overlap integral $\langle A|A - 1 \rangle$ and the spectroscopic factors, r.m.s.

radii $\langle r_{lj}^2 \rangle^{1/2} = \left(\int_0^\infty dr r^4 I_{lj}^2(r) / \int_0^\infty dr r^2 I_{lj}^2(r) \right)^{1/2}$ and single-particle ANCs $b_{lj} = C_{lj} / S_{lj}^{1/2}$ associated with it. We show them in Table II as well.

For proton unbound states we have calculated both the widths Γ_{lS}^0 and Γ_{lS} which are shown in Table III together with experimentally measured widths. Γ_{lS}^0 slightly depends on the choice of the channel radius a . We tried to choose this radius to be large enough, between 8.0 and 10.0 fm. In this region, the sensitivity of Γ_{lS}^0 to a is about 2% for narrow resonances but can reach about 7% for broad s -wave resonances. The coefficient $\alpha = \Gamma_{lS} / \Gamma_{lS}^0$ that connects Γ_{lS} and Γ_{lS}^0 is also a -dependent so that the sensitivity of Γ_{lS} to the choice of a decreases. These coefficients, shown in Table III, are between 1.01 and 1.05 for narrow resonances but can increase up to 1.38 for broad s -wave resonances.

The averaged over two NN potentials ratios $\mathcal{R}_{\Gamma_0}^{MCM}$ and $\mathcal{R}_{\Gamma}^{MCM}$ are shown in Table IV together with the analytical estimate $\mathcal{R}_{\Gamma_0}^{MCM}$ and the single-particle estimate $\mathcal{R}_{\Gamma}^{s.p.}$. The ratios $\mathcal{R}_{\Gamma_0}^{MCM} / \mathcal{R}_0^{res}$ and $\mathcal{R}_{\Gamma}^{MCM} / \mathcal{R}_{\Gamma}^{s.p.}$ are also presented in Fig. 4.

1. $^8\text{B} - ^8\text{Li}$

According to Table II, the ANCs in small $j = 1/2$ components of the $\langle ^8\text{Li}|^7\text{Li} \rangle$ overlap integral strongly depend on the choice of the NN potential. However, in dominant components $j = 3/2$ they are very similar. The total neutron ANC squared C_1^2 are practically the same for both the NN potentials used in calculations. The total widths $\Gamma_l = \sum_S \Gamma_{lS}$ are also practically the same for both V2 and MN (see Table III). The ratio $\mathcal{R}_{\Gamma_0}^{MCM}$ varies within 5% with the NN potential choice. Its average value of

TABLE II: Asymptotic normalization coefficients squared C_{lj}^2 (in fm^{-1}), spectroscopic factors S_{lj} , single-particle ANCs squared $b_{lj}^2 = C_{lj}^2/S_{lj}$ (in fm^{-1}) and r.m.s. radii $\langle r_{lj}^2 \rangle^{1/2}$ (in fm) for the nuclei from the first column. The calculations have been performed with two NN potentials, V2 and MN. The experimental neutron separation energies have been reproduced.

Nucleus	lj	V2				MN			
		C_{lj}^2	S_{lj}	b_{lj}^2	$\langle r_{lj}^2 \rangle^{1/2}$	C_{lj}^2	S_{lj}	b_{lj}^2	$\langle r_{lj}^2 \rangle^{1/2}$
${}^8\text{Li}(1^+)$	$p_{1/2}$	0.0135	0.051	0.263	4.43	0.0255	0.097	0.263	4.42
	$p_{3/2}$	0.1378	0.514	0.268	4.46	0.1261	0.525	0.240	4.30
	total	0.1513	0.566			0.1516	0.622		
${}^{12}\text{B}(2^+)$	$p_{1/2}$	0.536	0.490	1.10	3.79	0.490	0.500	0.979	3.68
	$p_{3/2}$	0.0235	0.0177	1.33	3.99	0.0202	0.0143	1.412	4.06
	total	0.560	0.507			0.510	0.514		
${}^{12}\text{B}(0^+)$	$p_{3/2}$	0.0835	0.607	0.138	4.77	0.0638	0.515	0.124	4.57
${}^{12}\text{B}(2^-)$	$s_{1/2}$	2.721	0.898	3.03	4.99	2.504	0.934	2.68	4.78
${}^{12}\text{B}(1^-)$	$s_{1/2}$	1.292	1.016	1.27	6.49	1.148	0.992	1.158	6.25
${}^{13}\text{C}(\frac{1}{2}^+)^{2c}$	$s_{1/2}$	3.46 ± 0.02	0.94	3.70 ± 0.02	4.98	3.41 ± 0.03	1.04	3.28 ± 0.02	4.80
${}^{13}\text{C}(\frac{1}{2}^+)^{4c}$	$s_{1/2}$	3.39 ± 0.02	0.94	3.60 ± 0.01	4.98	2.77 ± 0.03	0.92	3.01 ± 0.03	4.77
${}^{13}\text{C}(\frac{3}{2}^-)^{2c}$	$p_{3/2}$	0.0992	0.271	0.365	4.21	0.0931	0.283	0.331	4.09
${}^{13}\text{C}(\frac{3}{2}^-)^{4c}$	$p_{3/2}$	0.129 ± 0.001	0.370	0.350 ± 0.002	4.18	0.100 ± 0.002	0.363	0.274 ± 0.004	3.90
${}^{13}\text{C}(\frac{5}{2}^+)^{2c}$	$d_{5/2}$	0.0272	0.881	0.031	4.04	0.0222	0.873	0.025	3.86
${}^{13}\text{C}(\frac{5}{2}^+)^{4c}$	$d_{5/2}$	0.0213 ± 0.0006	0.81	0.0263 ± 0.0006	3.90	0.0153 ± 0.0003	0.84	0.0183 ± 0.0004	3.59
${}^{23}\text{Ne}(\frac{1}{2}^+)^a$	$s_{1/2}$	3.52	0.202	17.4	4.31	2.37	0.154	15.4	4.19
${}^{23}\text{Ne}(\frac{1}{2}^+)^b$	$s_{1/2}$	18.49	1.08	17.1	4.26	16.3	1.08	15.0	4.12
${}^{27}\text{Mg}(\frac{3}{2}^+)^a$	$d_{3/2}$	1.89 ± 0.03	0.744 ± 0.002	2.54 ± 0.03	3.63	0.695 ± 0.012	0.318 ± 0.002	2.18 ± 0.02	3.56
${}^{27}\text{Mg}(\frac{3}{2}^+)^b$	$d_{3/2}$	2.61 ± 0.04	1.08	2.43 ± 0.03	3.60	2.03 ± 0.04	1.08	1.88 ± 0.04	3.47

^{2c} - two-cluster model

^{4c} - four-cluster model

^{a)} - multi-channel cluster model

^{b)} - single-channel cluster model

$(1.80 \pm 0.04) \times 10^{-3}$ is about 10 % smaller than the prediction $\mathcal{R}_0^{res} = (2.06 \pm 0.04) \times 10^{-3}$ of the analytical formula (2). The ratio $\mathcal{R}_\Gamma^{MCM} = (1.73 \pm 0.03) \times 10^{-3}$ is close to the single-particle estimate $\mathcal{R}_\Gamma^{s.p.} = (1.78 \pm 0.01) \times 10^{-3}$.

The neutron ANCs for ${}^8\text{Li}(1^+)$ have been determined from experimental study of the transfer reaction ${}^{13}\text{C}({}^7\text{Li}, {}^8\text{Li}){}^{12}\text{C}$ in Ref. [19]. It was found that $C_{1\frac{1}{2}}^2/C_{1\frac{1}{2}}^2 = 0.22(3)$ and $C_1^2 = 0.082 \pm 0.009$ fm. The measured ratio $C_{1\frac{1}{2}}^2/C_{1\frac{1}{2}}^2$ is in excellent agreement with our prediction of 0.20 with the MN force but is about twice as high as the prediction of 0.098 made with the V2 potential. The total value of the experimental ANC squared is significantly lower than the predictions of the MCM.

Two experimental values of the proton width Γ_l for the 1^+ resonance are available, 37 ± 5 keV from the ${}^7\text{Be}(p, \gamma){}^8\text{B}$ reaction [20] and 31 ± 4 keV from elastic scattering ${}^7\text{Be} + p$ [21]. The MCM calculations give larger widths, 50.9 keV and 52.7 keV for V2 and MN respectively. The ratio \mathcal{R}_Γ^{exp} , calculated with $\Gamma_l = 37 \pm 5$ keV, is $(2.29 \pm 0.28) \times 10^{-3} \hbar c$. This is significantly larger than the MCM value of $(1.73 \pm 0.03) \times 10^{-3} \hbar c$ obtained in this work (see Table IV). With more recent value, $\Gamma_l = 31 \pm 4$ keV, this ratio is smaller, $\mathcal{R}_\Gamma^{exp} = (1.92 \pm 0.23) \times 10^{-3} \hbar c$, and it agrees with $\mathcal{R}_\Gamma^{MCM} = (1.73 \pm 0.03) \times 10^{-3}$ within

the error bars.

2. ${}^{12}\text{B} - {}^{12}\text{N}$

The ANCs squared obtained for the 2^+ , 2^- and 1^- states of ${}^{12}\text{B}$ with V2 and MN differ by 9-13% from each other. For ${}^{12}\text{B}(0^+)$ this difference is larger, about 30%. The neutron spectroscopic factors change by 1-6% with different choices of the NN potential except for 0^+ , where this difference reaches 18%. The proton widths in ${}^{12}\text{N}$ differ by 6-9% for the 2^+ , 2^- and 1^- states and by 32% for the 0^+ state. The sensitivity of the calculated ratios $\mathcal{R}_{\Gamma_0}^{MCM}$ and \mathcal{R}_Γ^{MCM} to the NN potential is less than 3% except for the broad resonance 1^- where it reaches 6%.

The average value of \mathcal{R}_Γ^{MCM} is lower than the analytical estimate \mathcal{R}_0^{res} by 15%, 18%, 28% and 16% for the 2^+ , 0^+ , 2^- and 1^- states respectively. The other ratio, \mathcal{R}_Γ^{MCM} compares with the single-particle estimate $\mathcal{R}_\Gamma^{s.p.}$ in a different way for each state. For the narrow resonance 2^+ , they agree within 2%. For the resonance 0^+ , which is broad in the single-particle potential model ($\Gamma_l \sim 0.7$ MeV) but is much narrower in the MCM ($\Gamma_l \sim 0.3$ MeV), $\mathcal{R}_\Gamma^{s.p.}$ is larger than the analyt-

TABLE III: The proton widths Γ_{lS}^0 , Γ_{lS} (in keV) and the coefficient $\alpha = \Gamma_{lS}^0/\Gamma_{lS} = 1 + \gamma_{lS}^2 S'_l$ that relates them (see Eq. (20), for the resonances from the first column. Also shown are the resonance energies E_{res} (in keV), orbital momenta l and channel radii a (in fm). For the resonances $^8\text{B}(1^+)$ and $^{12}\text{N}(2^+)$ two values of channel spin S are possible. The proton widths in these channels are shown separately. The calculations have been performed with two NN potentials, V2 and MN.

Resonance	E_{res}	l	a	V2			MN			Γ_p^{exp}
				Γ_{lS}^0	α	Γ_{lS}	Γ_{lS}^0	α	Γ_{lS}	
$^8\text{B}(1^+)$	633	1	10.0	$S=1$	42.4	1.042	40.7	49.8	1.050	47.4
				$S=2$	10.3	1.010	10.2	5.36	1.005	5.33
				total			50.9			52.7
$^{12}\text{N}(2^+)$	359	1	8.55	$S=1$	0.949	1.032	0.920			
				$S=2$	0.388	1.013	0.383			
				total			1.30			< 20 [23]
				8.75				0.879	1.028	0.855
					$S=1$			0.365	1.011	0.361
$^{12}\text{N}(0^+)$	1839	1	8.55							< 20 [23]
					344	1.034	332	260	1.026	253
										68 ± 21 [23]
$^{12}\text{N}(2^-)$	589	0	8.75		150	1.26	119	138	1.24	111
$^{12}\text{N}(1^-)$	1199	0	8.55					771	1.108	696
				8.75						750 ± 250 [23]
$^{13}\text{N}(\frac{1}{2}^+)^{2c}$	422	0	8.5		821	1.109	740			
				9.5	50.4	1.30	38.8	46.3	1.25	37.0
					51.2	1.38	37.1	43.4	1.32	32.8
$^{13}\text{N}(\frac{1}{2}^+)^{4c}$	422	0	8.0	8.5	49.3	1.33	37.1	41.6	1.28	32.6
				9.5	118	1.021	116	114	1.020	112
				9.5	116	1.015	114	112	1.014	110
$^{13}\text{N}(\frac{3}{2}^-)^{4c}$	1557	1	8.5	164	1.028	159	132	1.023	129	62 \pm 4 [24]
				8.9	160	1.024	156	128	1.020	126
				8.5	69.5	1.046	66.4	57.1	1.038	55.0
$^{13}\text{N}(\frac{5}{2}^+)^{2c}$	1607	2	8.5	9.5	68.0	1.031	66.0	55.8	1.025	54.4
				8.0	57.4	1.046	54.9	41.3	1.033	40.0
				8.5	56.0	1.037	54.0	39.6	1.026	38.6
$^{23}\text{Al}(\frac{1}{2}^+)^a$	405	0	9.0		2.01×10^{-2}	1.015	1.98×10^{-2}	1.26×10^{-2}	1.010	1.25×10^{-2}
$^{23}\text{Al}(\frac{1}{2}^+)^b$	405	0	9.0		9.19×10^{-2}	1.071	8.58×10^{-2}	8.19×10^{-2}	1.063	7.70×10^{-2}
$^{27}\text{P}(\frac{3}{2}^+)^a$	340	2	9.5		7.18×10^{-6}	1.003	7.16×10^{-6}	2.14×10^{-6}	1.001	2.14×10^{-6}
$^{27}\text{P}(\frac{3}{2}^+)^b$	340	2	9.5		1.04×10^{-5}	1.005	1.04×10^{-5}	8.26×10^{-6}	1.004	8.23×10^{-6}

^{2c} - two-cluster model

^{4c} - four-cluster model

^a) - multi-channel cluster model

^b) - single-channel cluster model

ical estimate \mathcal{R}_0^{res} (for most other cases it is smaller) and discrepancy between \mathcal{R}_Γ^{MCM} and $\mathcal{R}_\Gamma^{s.p.}$ is about 28%. For the relatively broad s -wave resonance 2^- , in which $\Gamma_l/E_R \sim 0.2$, this discrepancy is about 13%. For the broad s -wave resonance 1^- we have not succeeded to determine $\mathcal{R}_\Gamma^{s.p.}$ because in the single-particle potential model its width is comparable to the resonance width.

The neutron ANC s and r.m.s. radii for the $\langle ^{12}\text{B}(2^-)|^{11}\text{B}\rangle$ and $\langle ^{12}\text{B}(1^-)|^{11}\text{B}\rangle$ overlap integrals have been reported in Ref. [22] where they have been determined from the $^{11}\text{B}(\text{d},\text{p})^{12}\text{B}$ reaction. The experimental

values of C_1^2 are 1.80 ± 0.32 fm $^{-1}$ and 0.88 ± 0.15 fm $^{-1}$ for the 2^- and 1^- respectively. They are about 30 to 50% lower than the predictions of the MCM.

The experimental value of the r.m.s. radius for 2^- , $\langle r_{exp}^2 \rangle^{1/2} = 4.01 \pm 0.61$ fm from Ref. [22], is lower than the MCM predictions $\langle r^2 \rangle^{1/2} = 4.99$ and 4.78 fm, while for the 1^- state our predictions, 6.49 fm and 6.25 fm, agree with the experimental value $\langle r_{exp}^2 \rangle^{1/2} = 5.64 \pm 0.90$ fm within the error bars.

Using the experimentally measured ANC s for $^{12}\text{B}(2^-)$ and $^{12}\text{B}(1^-)$ and the widths of the $^{12}\text{N}(2^-)$ and $^{12}\text{N}(1^-)$

TABLE IV: Ratios $\mathcal{R}_{\Gamma_0}^{MCM}$ and $\mathcal{R}_{\Gamma}^{MCM}$ obtained in the MCM in comparison with the prediction \mathcal{R}_0^{res} of the analytical formula (2) and single-particle estimate $\mathcal{R}_{\Gamma}^{s.p.}$ (all given in units of $\hbar c$) for the mirror pairs from the first column. Also shown are spins and parities J^{π} of the mirror states and orbital momenta l of the relative motion in the resonance. The results of the MCM calculations are averaged over two NN potentials. For ^{13}N , Γ_{IS}^0 obtained with a larger value of a is used to calculate $\mathcal{R}_{\Gamma_0}^{MCM}$.

Mirror pair	J^{π}	l	$\mathcal{R}_{\Gamma_0}^{MCM}$	\mathcal{R}_0^{res}	$\mathcal{R}_{\Gamma}^{MCM}$	$\mathcal{R}_{\Gamma}^{s.p.}$
^8Li - ^8B	1^+	1	$(1.80 \pm 0.04) \times 10^{-2}$	$(2.06 \pm 0.04) \times 10^{-2}$	$(1.73 \pm 0.03) \times 10^{-2}$	$(1.78 \pm 0.01) \times 10^{-2}$
^{12}B - ^{12}N	2^+	1	$(1.22 \pm 0.02) \times 10^{-5}$	$(1.43 \pm 0.01) \times 10^{-5}$	$(1.20 \pm 0.02) \times 10^{-5}$	1.22×10^{-5}
^{12}B - ^{12}N	0^+	1	$(2.07 \pm 0.02) \times 10^{-2}$	$(2.51 \pm 0.05) \times 10^{-2}$	2.01×10^{-2}	$(2.77 \pm 0.14) \times 10^{-2}$
^{12}B - ^{12}N	2^-	0	2.79×10^{-4}	$(3.83 \pm 0.31) \times 10^{-4}$	$(2.23 \pm 0.02) \times 10^{-4}$	$(2.55 \pm 0.08) \times 10^{-4}$
^{12}B - ^{12}N	1^-	0	$(3.31 \pm 0.09) \times 10^{-3}$	$(3.97 \pm 0.56) \times 10^{-3}$	$(2.98 \pm 0.08) \times 10^{-3}$	
^{13}C - $^{13}\text{N}^{2c}$	$\frac{1}{2}^+$	0	$(7.13 \pm 0.11) \times 10^{-5}$	$(9.64 \pm 0.81) \times 10^{-5}$	$(5.59 \pm 0.21) \times 10^{-5}$	$(6.21 \pm 0.25) \times 10^{-5}$
^{13}C - $^{13}\text{N}^{4c}$	$\frac{1}{2}^+$	0	$(7.49 \pm 0.12) \times 10^{-5}$	$(9.64 \pm 0.81) \times 10^{-5}$	$(5.77 \pm 0.22) \times 10^{-5}$	$(6.21 \pm 0.25) \times 10^{-5}$
^{13}C - $^{13}\text{N}^{2c}$	$\frac{3}{2}^-$	1	$(6.01 \pm 0.09) \times 10^{-3}$	$(7.64 \pm 0.06) \times 10^{-3}$	$(5.96 \pm 0.08) \times 10^{-3}$	$(6.98 \pm 0.22) \times 10^{-3}$
^{13}C - $^{13}\text{N}^{4c}$	$\frac{3}{2}^-$	1	$(6.39 \pm 0.10) \times 10^{-3}$	$(7.64 \pm 0.06) \times 10^{-3}$	$(6.32 \pm 0.14) \times 10^{-3}$	$(6.98 \pm 0.22) \times 10^{-3}$
^{13}C - $^{13}\text{N}^{2c}$	$\frac{5}{2}^+$	2	1.27×10^{-2}	$(1.43 \pm 0.01) \times 10^{-2}$	$(1.24 \pm 0.01) \times 10^{-2}$	$(1.37 \pm 0.03) \times 10^{-2}$
^{13}C - $^{13}\text{N}^{4c}$	$\frac{5}{2}^+$	2	$(1.32 \pm 0.01) \times 10^{-2}$	$(1.43 \pm 0.01) \times 10^{-2}$	1.30×10^{-2}	$(1.37 \pm 0.03) \times 10^{-2}$
^{23}Ne - $^{23}\text{Al}^a$	$\frac{1}{2}^+$	0	$(2.79 \pm 0.10) \times 10^{-8}$	$(3.22 \pm 0.13) \times 10^{-8}$	$(2.76 \pm 0.09) \times 10^{-8}$	$(2.69 \pm 0.02) \times 10^{-8}$
^{23}Ne - $^{23}\text{Al}^b$	$\frac{1}{2}^+$	0	$(2.53 \pm 0.02) \times 10^{-8}$	$(3.22 \pm 0.13) \times 10^{-8}$	$(2.44 \pm 0.09) \times 10^{-8}$	$(2.69 \pm 0.02) \times 10^{-8}$
^{26}Mg - $^{27}\text{P}^a$	$\frac{3}{2}^+$	2	$(1.75 \pm 0.19) \times 10^{-11}$	2.21×10^{-11}	$(1.76 \pm 0.18) \times 10^{-11}$	$(2.25 \pm 0.10) \times 10^{-11}$
^{26}Mg - $^{27}\text{P}^b$	$\frac{3}{2}^+$	2	$(2.04 \pm 0.02) \times 10^{-11}$	2.21×10^{-11}	$(2.04 \pm 0.02) \times 10^{-11}$	$(2.25 \pm 0.10) \times 10^{-11}$

^{2c} - two-cluster model

^{4c} - four-cluster model

^{a)} - multi-channel cluster model

^{b)} - single-channel cluster model

resonances from Ref. [23], we obtain $\mathcal{R}_{\Gamma}^{exp} = (3.32 \pm 0.98) \times 10^{-4} \hbar c$ and $(4.3 \pm 2.2) \times 10^{-3} \hbar c$ for the 2^- and 1^- states respectively. For the 2^- resonance, the experimental value $\mathcal{R}_{\Gamma}^{exp}$ is larger than the theoretical ratio $(2.23 \pm 0.02) \times 10^{-4} \hbar c$. For the 1^- state, the error bars of $\mathcal{R}_{\Gamma}^{exp}$ are too large to make conclusive judgement about the agreement with theoretical calculations.

3. ^{13}C - ^{13}N

We have used two different models to describe the mirror pair ^{13}N - ^{13}C : the multichannel two-cluster model ^{12}C + n(p) of Ref. [17] and the multichannel four-cluster model $\alpha + \alpha + \alpha + \text{n(p)}$ from Ref. [18]. The difference between these two models in predictions of ANC_s, spectroscopic factors and proton widths reaches sometimes 30% or more (see Tables II and III). In our previous work [5], the two- and four-cluster calculations gave even larger difference in mirror ANC_s of ground states of the mirror pair ^{13}N - ^{13}C . As explained in Ref. [5], such a large difference arises because the $\alpha + \alpha + \alpha$ model for the remnant nucleus ^{12}C , used in the four-cluster calculations, contains only one type of the permutational symmetry, namely, the one determined by the Young diagrams [f] = [444]. One-center shell model of ^{12}C , used in the two-cluster calculations, contains all the other types of permutational symmetry which may give significant contributions to nuclear properties associated with one nucleon

removal.

The sensitivity of the ANC_s squared and the proton widths on the NN potential choice is different for each mirror pair of excited states, however is does not exceed 30%. Dependence of the ratio $\mathcal{R}_{\Gamma_0}^{MCM}$ or $\mathcal{R}_{\Gamma}^{MCM}$ on the NN potential is weaker, less than 5% for the $\frac{3}{2}^-$ and $\frac{5}{2}^+$ states and 7% for the $\frac{1}{2}^-$ state.

The calculated ratio $\mathcal{R}_{\Gamma_0}^{MCM}$ is smaller than the analytical estimate \mathcal{R}_0^{res} by 8 to 22% for narrow resonances $\frac{3}{2}^-$ and $\frac{5}{2}^+$ and by 32% for the wide s -wave resonance $\frac{1}{2}^+$. The other ratio, $\mathcal{R}_{\Gamma}^{MCM}$, compares with the single-particle estimate $\mathcal{R}_{\Gamma}^{s.p.}$ more favourably, it is smaller than $\mathcal{R}_{\Gamma}^{s.p.}$ by 6 to 15%.

The neutron ANC_s and r.m.s. radii for the $\langle ^{13}\text{C}(\frac{1}{2}^+) | ^{12}\text{C} \rangle$ and $\langle ^{13}\text{C}(\frac{5}{2}^+) | ^{12}\text{C} \rangle$ overlap integrals have been reported in Ref. [22] where they have been determined from the $^{12}\text{C}(\text{d},\text{p})^{13}\text{C}$ reaction. The experimental values of C^2 are $3.39 \pm 0.59 \text{ fm}^{-1}$ and $0.023 \pm 0.003 \text{ fm}^{-1}$ for the $\frac{1}{2}^+$ and $\frac{5}{2}^+$ respectively. For $\frac{1}{2}^+$, the ANC squared $C^2 = 3.65 \pm 0.34$ (statistical error) ± 0.35 (systematic error) fm^{-1} has been independently measured in Ref. [25] using the same reaction. This value is slightly larger than the one from Ref. [22] but agrees with it within the error bars. The four-cluster MCM calculations with V2 potential and the two-cluster calculations with both NN potentials give for C^2 the values of 3.39, 3.46 and 3.41 fm^{-1} that agree with the experimentally

measured one. The four-cluster calculations with MN give slightly smaller ANC squared, 2.77 fm^{-1} . As for the $\frac{5}{2}^+$ state, only the two-cluster calculations with MN and the four-cluster calculations with V2, $C^2 = 0.0222 \text{ fm}^{-1}$ and $C^2 = 0.0213 \text{ fm}^{-1}$ respectively, agree with the experimentally determined value. The other two calculations either overestimate or underestimate it.

The experimental value of the r.m.s. radii, $\langle r_{exp}^2 \rangle^{1/2} = 5.04 \pm 0.75 \text{ fm}$ and $\langle r_{exp}^2 \rangle^{1/2} = 3.68 \pm 0.40 \text{ fm}$ for the $\frac{1}{2}^+$ and $\frac{5}{2}^+$ states in ^{13}C respectively, have been reported in Ref. [22]. They agree with the MCM predictions obtained both in two- and four-cluster model with V2 and MN potentials within the error bars.

Using the ANCs measured in Ref. [22, 25] for the $\frac{1}{2}^+$ and $\frac{5}{2}^+$ states in ^{13}C and the experimental proton widths for their mirror analogs available in Ref. [24], we can construct the ratio $\mathcal{R}_{\Gamma}^{exp} = \Gamma_p^{exp}/(C_n^{exp})^2$. For $\frac{1}{2}^+$, this ratio is $(4.74 \pm 0.94) \times 10^{-5} \hbar c$ or $(4.40 \pm 0.94) \times 10^{-5} \hbar c$ depending on whether the neutron ANC used is taken from Ref. [22] or [25]. The MCM ratios $\mathcal{R}_{\Gamma}^{MCM}$ of $(5.77 \pm 0.22) \times 10^{-5} \hbar c$ and $(5.59 \pm 0.21) \times 10^{-5} \hbar c$, obtained in four- and two-cluster calculations respectively, agree with the first value for $\mathcal{R}_{\Gamma}^{exp}$ within the error bars but are larger than the second value. As for the $\frac{5}{2}^+$ state, all the MCM calculations of the ratio $\mathcal{R}_{\Gamma}^{MCM}$ agree within the error bars with $\mathcal{R}_{\Gamma}^{exp} = (1.04 \pm 0.29) \times 10^{-2} \hbar c$, obtained using the experimental proton width of from [24] and the neutron ANC from [22].

4. $^{23}\text{Al} - ^{23}\text{Ne}$

The calculated ANCs and spectroscopic factors for $^{23}\text{Ne}(\frac{1}{2}^+)$ as well as the proton widths of $^{23}\text{Al}(\frac{1}{2}^+)$ are strongly influenced by the excitations in the ^{22}Ne and ^{22}Mg cores. Including the core excitations decrease C_l^2 , S_l and Γ_p by 4 to 7 times. Dependence of these values on the NN potential choice is much weaker, $\sim 12\%$ in the single-channel calculations and $\sim 50\%$ in the multi-channel calculations. The dependence of the ratio $\mathcal{R}_{\Gamma_0}^{MCM}$ on the NN potential is even weaker, 2% for single-channel calculations and 7% for multi-channel calculations. For $\mathcal{R}_{\Gamma}^{MCM}$, this dependence is about 7%. The core excitations lead to a 10% increase in $\mathcal{R}_{\Gamma_0}^{MCM}$ and a 13% increase in $\mathcal{R}_{\Gamma}^{MCM}$.

The MCM ratio $\mathcal{R}_{\Gamma_0}^{MCM}$ is about 20% lower than the predictions \mathcal{R}_0^{res} of the analytical formula (2). The other ratio, $\mathcal{R}_{\Gamma}^{MCM}$, is very close to the single-particle estimate $\mathcal{R}_{\Gamma}^{s.p.}$, if it is calculated with core excitations taken into account. Without taking core excitations into account, it is 10% smaller than $\mathcal{R}_{\Gamma}^{s.p.}$.

5. $^{27}\text{P} - ^{27}\text{Mg}$

As in the case of $^{23}\text{Ne} - ^{23}\text{Al}$, the MCM predictions strongly depend on whether the core excitations are taken into account or not. Without core excitations, the dependence of ANCs squared and proton widths on the NN potential choice is relatively weak, about 30%. When the core excitations are included, the spectroscopic factor for the $\langle ^{27}\text{Mg}(\frac{3}{2}^+) | ^{26}\text{Mg}(\text{g.s.}) \rangle$ overlap drops by 30% and 70% for the V2 and MN potential respectively. The C^2 and Γ_p values decrease approximately by the same amount too. Their dependence on the NN potential becomes much stronger, about 3 times.

The dependence of the ratio $\mathcal{R}_{\Gamma_0}^{MCM}$ and $\mathcal{R}_{\Gamma}^{MCM}$ on the NN potential in single-channel calculations is about 2%, but in the multichannel calculations this dependence increases up to 20%. In both cases, C^2 and Γ_p are more sensitive to the NN potential than their ratio.

The single-channel calculations of $\mathcal{R}_{\Gamma_0}^{MCM}$ and $\mathcal{R}_{\Gamma}^{MCM}$ are close to \mathcal{R}_0^{res} and $\mathcal{R}_{\Gamma}^{s.p.}$. The core excitations decrease $\mathcal{R}_{\Gamma_0}^{MCM}$ and $\mathcal{R}_{\Gamma}^{MCM}$ by about 15%.

VI. MIRROR SYMMETRY IN SPECTROSCOPIC FACTORS

Spectroscopic factors are often used to predict the widths of proton resonances in approaches of a shell model type. Two questions concerning this procedure arise: how reliable are the concepts of spectroscopic factors for unbound states and is there any mirror symmetry between such spectroscopic factors and their mirror analogs. In this section, we briefly address these questions from the point of view of the MCM.

The spectroscopic factor S_{lj} for a particle-bound state is defined as

$$S_{lj} = A \int_0^{\infty} dr r^2 (I_{lj}(r))^2, \quad (25)$$

where $I_{lj}(r)$ is a radial part of the overlap integral between the wave functions of nuclei A and $A - 1$. For unbound states, the contribution from the oscillating tail of this integral will lead to a divergent result for S_{lj} . In order to use the concept of the spectroscopic factor for unbound states, its definition should be modified. In the present paper, we define it as the norm of the overlap integral $I^{BSA}(r)$ between the wave function of nucleus A obtained in the bound state approximation and the wave function of nucleus $A - 1$.

The calculated proton overlap integrals decrease very slowly inside the channel radius a . For $l \neq 0$ resonances in the $0p$ -shell nuclei, the function $r I^{BSA}(r)$ typically decrease from its maximum value only by a factor of two or three. It decreases even slower for the s -wave resonance $^{13}\text{N}(\frac{1}{2}^+)$. We would like to note here that such a slow decrease is absent in shell model approaches. For very narrow sd -shell resonances $^{23}\text{Al}(\frac{1}{2}^+)$ and $^{27}\text{P}(\frac{3}{2}^+)$ with the

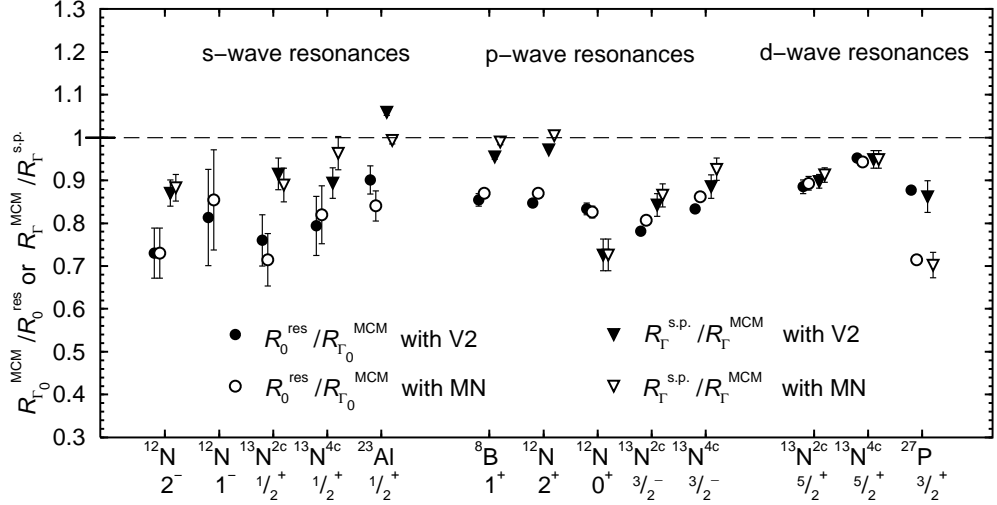


FIG. 4: Ratio between the MCM calculations $\mathcal{R}_{\Gamma_0}^{MCM}$ and the predictions \mathcal{R}_0^{res} of the analytical formula (2) and ratio between $\mathcal{R}_{\Gamma_0}^{MCM}$ and the single-particle estimate $\mathcal{R}_{\Gamma}^{s.p.}$. Both are calculated with two NN potentials, V2 and MN. Core excitations are taken into account and charge symmetry of NN interactions is broken. Both four-cluster (4c) and two-cluster (2c) calculations for ^{13}N are shown.

widths of $\sim 10^{-2}$ and $\sim 10^{-6}$ keV the strong Coulomb barrier traps their wave functions inside the channel radius so that $rI^{BSA}(r)$ decreases from its maximum value by an order of magnitude. This resembles more the conventional bound state behaviour of the wave functions so that shell model description for these states should be more adequate.

The calculated spectroscopic factors depend on the choice of the channel radius. We have performed the calculations for ^{13}N with two channel radii shown in Table III. Also, for ^{27}P , the calculations have been performed with $a = 9.0$ and 9.5 fm. The change in spectroscopic factors is less than 4% in all these cases. The ratio S_p/S_n between the mirror spectroscopic factors, calculated with larger value of a when available, is presented in Fig. 5. This figure shows significant symmetry breaking in spectroscopic factors, which $\sim 20\%$ for s -wave resonances and in $^{13}\text{N}(^{3-})$, $\sim 5\text{-}8\%$ for ^8B , $^{12}\text{N}(2^+)$, $^{12}\text{N}(0^+)$ and $^{13}\text{N}(^{5+})$, and for ^{27}P the charge symmetry breaking depends of the NN potential used in caluclations: it is $\sim 4\%$ for V2 and $\sim 25\%$ for MN. This is larger than the 3-9% charge-symmetry breaking in spectroscopic factors for bound-bound mirror pairs obtained in Ref. [5].

VII. SUMMARY AND CONCLUSIONS

Due to the charge symmetry of NN interactions the width of a narrow proton resonance is related to the ANC of its mirror neutron bound state. This relation (the ratio \mathcal{R}_{Γ}) can be approximated by a simple analytical formula (2) derived in Ref. [3]. In this paper, we have clarified that the width that enters formula (2) has the meaning of a residue in the R-matrix pole. In most cases, however, the widths that have been determined from experimental

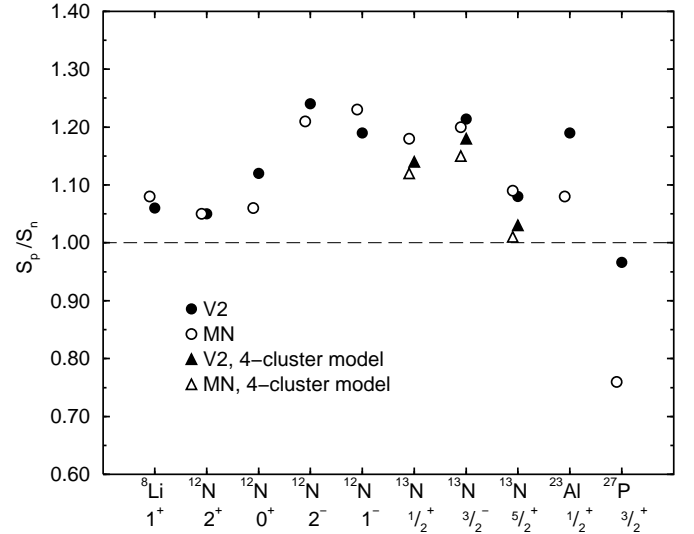


FIG. 5: Ratio between the proton and mirror neutron spectroscopic factors calculated within the MCM. For the ^{13}N - ^{13}C mirror pair, the circles represent the calculations obtained within the two-cluster MCM.

data are associated with Breit-Wigner shapes of the resonant cross sections. The MCM calculations, performed in this paper for a range of nuclei, have shown that these two widths can differ by less than 7% for narrow resonances and up to 30% for broad s -wave resonances. Since the most interesting applications of \mathcal{R}_{Γ} , for example, predictions of resonant proton capture rates using mirror neutron ANCs, require a knowledge of “observed” widths, investigation of a link between such “observed” widths with mirror neutron ANCs is also important.

In the present paper we have studied the ratio \mathcal{R}_{Γ} within the MCM. The calculated MCM proton widths

and neutron ANCs are very sensitive to the details of the model and to the NN interaction choice, however, the ratios $\mathcal{R}_{\Gamma_0}^{MCM}$ and $\mathcal{R}_{\Gamma}^{MCM}$, based on two different definitions of widths, are in most cases almost model-independent. Comparison of the ratio $\mathcal{R}_{\Gamma_0}^{MCM}$, associated with the residue in the R-matrix pole, with the predictions \mathcal{R}_0^{res} of Eq. (2) has confirmed the general trend in its behaviour given by this formula. The difference between $\mathcal{R}_{\Gamma_0}^{MCM}$ and \mathcal{R}_0^{res} are on average about 20% (see Fig.4) and does not exceed 30% for the range of nuclei considered here. This difference is larger than the average 6% divergence between the ratio of mirror ANCs for bound-bound mirror pairs obtained in the MCM for the same nuclei and its analytical estimate [5]. The other ratio, $\mathcal{R}_{\Gamma}^{MCM}$, associated with “observed widths”, is close to the estimate $\mathcal{R}_{\Gamma}^{s.p.}$, made in the single-particle model on the assumptions that mirror single-particle potential well are exactly the same. The average deviation between $\mathcal{R}_{\Gamma}^{MCM}$ and $\mathcal{R}_{\Gamma}^{s.p.}$ is about 10% and does not exceed 30% (see Fig.4). The large deviation, about 30%, obtained for the ^{27}Mg - ^{27}P mirror pair with the MN potential, can be explained by the restricted model space used to generate the wave functions of the ^{26}Mg and ^{26}Si cores. Let us note that $\mathcal{R}_{\Gamma}^{MCM}$ is close to $\mathcal{R}_{\Gamma}^{s.p.}$ even for broad s-wave resonances.

For few resonances, $^{8}\text{B}(1^+)$, $^{12}\text{N}(2^-, 1^-)$ and $^{13}\text{N}(\frac{1}{2}^+, \frac{5}{2}^+)$, the comparison of the ratio $\mathcal{R}_{\Gamma}^{MCM}$ with the ratio $\mathcal{R}_{\Gamma}^{exp}$ between experimentally measured widths and mirror neutron ANCs squared has been possible. We have observed agreement within the error bars between $\mathcal{R}_{\Gamma}^{MCM}$ and $\mathcal{R}_{\Gamma}^{exp}$ for $^{8}\text{B}(1^+)$, when $\mathcal{R}_{\Gamma}^{exp}$ has been constructed using new value for Γ_p from Ref. [21]. Also, the agreement has been achieved for $^{12}\text{N}(1^-)$, $^{13}\text{N}(\frac{5}{2}^+)$ and for $^{13}\text{N}(\frac{1}{2}^+)$, when $\mathcal{R}_{\Gamma}^{exp}$ is calculated using neutron ANC from Ref. [22]. For $^{8}\text{B}(1^+)$, the ratio $\mathcal{R}_{\Gamma}^{exp}$ calculated with old value of Γ_p from Ref. [20] is

larger than $\mathcal{R}_{\Gamma}^{MCM}$. $\mathcal{R}_{\Gamma}^{exp}$ is also larger than $\mathcal{R}_{\Gamma}^{MCM}$ for $^{12}\text{N}(2^-)$. For $^{13}\text{N}(\frac{1}{2}^+)$, $\mathcal{R}_{\Gamma}^{exp}$ constructed with neutron ANC from [25] is smaller than $\mathcal{R}_{\Gamma}^{MCM}$. The disagreement between $\mathcal{R}_{\Gamma}^{MCM}$ and $\mathcal{R}_{\Gamma}^{exp}$ indicates that, in the first instance, it is necessary to remeasure neutron ANCs. Unlike $\mathcal{R}_{\Gamma}^{MCM}$, which does not depend strongly on model assumptions, $\mathcal{R}_{\Gamma}^{exp}$ is constructed using ANCs that are determined via theoretical analysis of some neutron removal reactions. The systematical errors of such an analysis, for example, due to uncertainty in optical potential choice or because of influence of breakup effects, may be as high as 30%. Uncertainties in proton widths are usually smaller, but as the case of $^{8}\text{B}(1^+)$ has shown, they can noticeably influence $\mathcal{R}_{\Gamma}^{exp}$.

The knowledge of \mathcal{R}_{Γ} can be used to predict proton widths if the mirror neutron ANCs are known. It can have important astrophysical application to predict the proton capture rates via the resonances for which $\Gamma_p < \Gamma_{\gamma}$. Our calculations have shown that for each resonance the different model assumptions and NN potentials give the deviation from the average value of $\mathcal{R}_{\Gamma}^{MCM}$ no more than 10%. This means that if neutron ANCs squared are measured with an accuracy of 10-20%, then the proton widths can be determined with the accuracy of 10-30%. This is better than the use of unreliable concept of spectroscopic factors in continuum and analysis of stripping reactions to unbound states for the same purposes.

Acknowledgements

T.N.K. is grateful to Professors R.C. Johnson, D. Baye and I.J. Thompson for useful discussions. Support from the UK EPSRC via grant GR/T28577 is greatfully acknowledged.

[1] L.D. Blokhintsev, I. Borbely and E.I. Dolinskii, Sov. J. Part. Nucl. **8**, 485 (1977).

[2] A.M.Mukhamedzhanov and R.E. Tribble, Phys. Rev. **C59**, 3418 (1999).

[3] N.K. Timofeyuk, R.C. Johnson and A.M. Mukhamedzhanov, Phys. Rev. Lett. **91**, 232501 (2003).

[4] C. Iliadis, L.Buchmann, P.M.Endt, H.Herndl, M.Wiescher, Phys. Rev. **C 53**, 475 (1996)

[5] N.K. Timofeyuk and P. Descouvemont, Phys. Rev. C **71**, 064305 (2005).

[6] A.I. Baz', Ya. B. Zel'dovich, and A.M. Peremolov, *Quantum Theory of Scattering and Reactions* (Nauka, Moscow, 1975)

[7] D. Baye, P. Descouvemont, Nucl. Phys. **A419**, 397 (1984) and Nucl. Phys. **A443**, 302 (1985)

[8] G.R. Satchler, *Direct Nuclear Reactions* (Oxford Press, New York, 1983)

[9] N.K. Timofeyuk, Nucl. Phys. **A632**, 38 (1998).

[10] A.M. Lane, R.G. Thomas, Rev. Mod. Phys. 30 (1958) 257.

[11] P. Descouvemont and M. Vincke Phys. Rev. **A 42**, 3835 (1990)

[12] A.B. Volkov, Nucl.Phys. **74**, 33 (1965).

[13] D.R. Thompson, M. LeMere and Y.C. Tang, Nucl. Phys. A286, 53 (1977).

[14] D. Baye and N. Pecher, Bull. Cl. Sc. Acad. Roy. Belg. **67** 835, (1981).

[15] P.Descouvemont, Phys. Rev **C 70**, 065802 (2004)

[16] P.Descouvemont, Nucl. Phys. **A646**, 261 (1999)

[17] N.K. Timofeyuk, D. Baye and P. Descouvemont, Nucl. Phys. **A620**, 29 (1997).

[18] M. Dufour and P. Descouvemont, Phys. Rev. **C 56**, 1831 (1997)

[19] L.Trache, A.Azhari, F.Carstoiu, H.L.Clark, C.A.Gagliardi, Y.-W.Lui, A.M.Mukhamedzhanov, X.Tang, N.Timofeyuk, R.E.Tribble, Phys.Rev. **C 67**, 062801(R) (2003)

[20] F. Ajzenberg-Selove, Nucl. Phys. **A490**, 1 (1988).

[21] C.Angulo, M.Azzouz, P.Descouvemont, G.Tabacaru,

D.Baye, M.Cogneau, M.Couder, T.Davinson, A.Di Pietro, P.Figuera, M.Gaelens, P.Leleux, M.Loiselet, A.Ninane, F.de Oliveira Santos, R.G.Pizzone, G.Ryckewaert, N.de Sereville, F.Vanderbist Nucl.Phys. **A716**, 211 (2003).

[22] Z.H. Liu, C.J. Lin, H.Q. Zhang, Z.C. Li, J.S. Zhang, Y.W. Wu, F. Yang, M. Ruan, J.C. Liu, S.Y. Li and Z.H. Peng, Phys. Rev. **C64**, 034312 (2001).

[23] F. Ajzenberg-Selove and J.H. Kelley, Nucl. Phys. A506, 1 (1990)

[24] F. Ajzenberg-Selove, Nucl. Phys. **A523**, 1 (1991).

[25] N. Imai, N.Aoi, S.Kubono, D.Beaumel, K.Abe, S.Kato, T.Kubo, K.Kumagai, M.Kurokawa, X.Liu, A.Mengoni, S.Michimasa, H.Ohnuma, H.Sakurai, P.Strasser, T.Teranishi, M.Ishihara Nucl. Phys. **A688**, 281c (2001).